RESEARCH ARTICLE | NOVEMBER 25 2024

Room temperature lasing from InGaAs quantum well nanowires on silicon-on-insulator substrates

Balthazar Temu ; Zhao Yan ; Bogdan-Petrin Ratiu ; Sang Soon Oh ; Qiang Li

Appl. Phys. Lett. 125, 223501 (2024)
https://doi.org/10.1063/5.0237589

Applied Physics Letters ARTICLE pubs.aip.org/aip/apl

Room temperature lasing from InGaAs quantum well nanowires on silicon-on-insulator substrates

Cite as: Appl. Phys. Lett. **125**, 223501 (2024); doi: 10.1063/5.0237589
Submitted: 5 September 2024 · Accepted: 7 November 2024 ·
Published Online: 25 November 2024

Balthazar Temu, Zhao Yan, Bogdan-Petrin Ratiu, Sang Soon Oh, and Qiang Li[a]

AFFILIATIONS

School of Physics and Astronomy, Cardiff University, Cardiff CF24 3AA, United Kingdom

[a]Author to whom correspondence should be addressed: LiQ44@cardiff.ac.uk

ABSTRACT

In this work we demonstrate room temperature lasing from core-shell nanowires consisting of a radial InGaAs quantum well as the active material. The nanowires with the GaAs/InGaAs/InGaP quantum well structures are arranged in a deformed honeycomb lattice, forming a photonic crystal surface emitting laser (PCSEL). We demonstrate lasing from devices with three different nanowire diameters from undeformed, stretched, and compressed honeycomb lattices. Under optical pumping we show that the PCSEL lases at the wavelength of 966 nm (stretched pattern), with the lasing threshold of 103 μJ/cm^2. The lasing wavelength increases as the nanowire diameter increases. Combining photoluminescence results and numerical simulations on the field profile and the quality factors of the devices, we establish that the lasing of the device is from the radial quantum well structure.

Nanowires can be used to make efficient laser sources for photonic integrated circuits applications.[1–3] Growing nanowires on silicon avoids any threading dislocations,[4,5] thanks to the lateral relaxation of strain facilitated by reduced contact area between the nanowire and the silicon substrate.[6,7] Introducing quantum confinement in the nanowires can enhance radiative recombination and make the resulting device even more energy efficient.[8] Quantum confinement in nanowires can be achieved in either radial or axial direction. Using vapor liquid solid (VLS) method,[9,10] multiple quantum disks in nanowires[11,12] were used to achieve quantum confinement in the axial direction where telecom band lasing was realized. Quantum confinement in the radial direction was also demonstrated by using quantum wells as the gain material, with the nanowires having a core-shell/core-multi shell structure.[13–16] However, the VLS method lacks precise control of the nanowire growth position and it is challenging to achieve high yield necessary for photonic crystal lasers. Catalyst free selective area epitaxy (SAE) via metal organic chemical vapor deposition (MOCVD) can circumvent these issues and enable nanowire photonic crystal arrays with versatile geometries.[17–22] Using this method, band edge photonic crystal lasers using the M point for emission were demonstrated.[23,24] Although nanowires grown by SAE often deploy a shell for surface passivation purpose,[25–29] achieving strained quantum wells in the radial direction is very challenging. In this work, we demonstrate photonic crystal surface emitting laser (PCSEL) using quantum well nanowires grown by SAE MOCVD method. The nanowires have a core-shell structure formed by a GaAs/InGaAs/InGaP radial quantum well. Although some nanowire based PCSELs have already been demonstrated,[30–33] to date there have been very few reports of nanowire PCSELs using radial quantum wells as the gain medium for lasing.

The nanowires in this work are grown on (111) oriented silicon-on-insulator (SOI) substrates using an AIXTRON close-coupled showerhead MOCVD system. To fabricate the nanohole pattern for subsequent SAE, a 20 nm layer of SiN mask was first deposited using plasma enhanced chemical vapor deposition (PECVD). Electron beam lithography and selective etching of the SiN mask was performed to expose the silicon underneath the SiN mask as shown in Fig. 1(a). Before growth, the patterned sample was cleaned using diluted hydrofluoric acid (HF) to remove any native oxide. The sample was then immediately transferred to the reactor. The reactor temperature was ramped up to 950 °C to remove any remaining oxide present on the silicon surface. The growth precursors used were triethylgallium (TEGa), trimethylindium (TMIn), tertiarybutylarsine (TBAs), and tertiarybutylphosphine (TBP). The reactor temperature was then reduced to 794 °C with the V/III ratio of 80 to grow GaAs core to the height of 800 nm on the nanohole location as shown in Fig. 1(b). The growth temperature was further reduced to 710 °C with the V/III ratio of 40 and an In/III vapor supply of 40% to grow the InGaAs layer

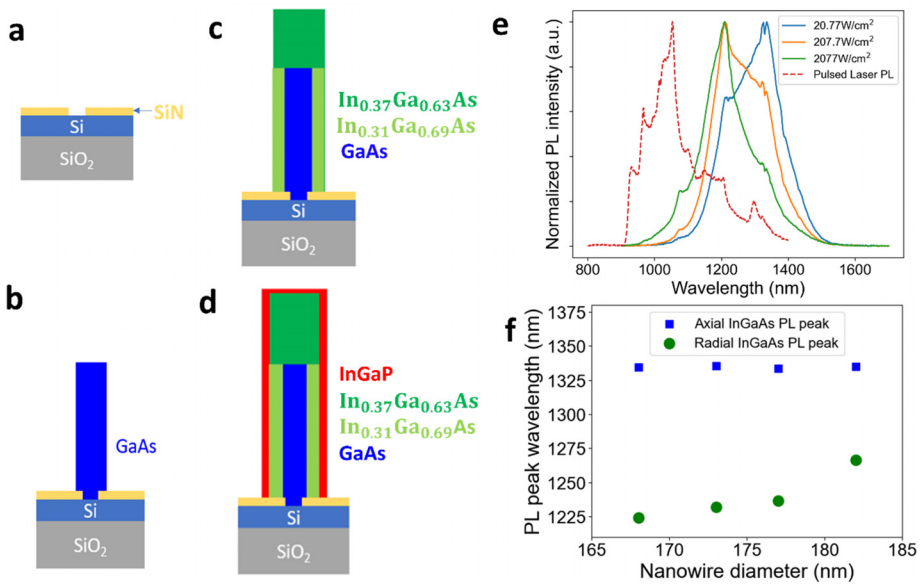

FIG. 1. Growth steps of the nanowires: (a) Nanohole made by electron beam lithography on SiN mask; (b) GaAs core grown on the nanohole; (c) the growth of InGaAs active material; (d) the growth of the InGaP passivation shell. (e) Room temperature PL spectra obtained by pumping with HeNe CW laser at different pumping powers (solid line) and PL spectrum obtained when the same sample is pumped with pulsed laser (dashed line). (f) Peak wavelengths of the PL spectrum plotted against nanowire diameters showing the axial InGaAs PL peak (blue squares) and radial InGaAs PL peak (green circles).

surrounding the GaAs core. The InGaAs grows simultaneously in both the axial ⟨111⟩ direction and in the radial direction, however, with different indium incorporation efficiency, as shown in Fig. 1(c). Previous TEM study[30] revealed a lower indium composition in the radial InGaAs (shown in light green) compared to the axial InGaAs (dark green). Finally, the reactor temperature was reduced to 660 °C to grow a 15 nm InGaP shell under a V/III ratio of 160 [see Fig. 1(d)]. The I nGaP shell helps to prevent non radiative recombination on the surface of the nanowire[26] by confining the carriers within the active I nGaAs layer.[27,28]

Figure 1(e) shows power dependent photoluminescence (PL) taken at room temperature using a HeNe CW laser (solid lines) and a pulsed laser (dashed line) as the pumping laser. Under the CW laser pumping, emission peaks from both the radial and axial InGaAs regions were observed. At a low pumping power of about 20.77 W/cm^2, the stronger PL peak was at 1335 nm presumably from the axial InGaAs region with a smaller bandgap. With the pumping power increased up to 2077 W/cm^2, while the whole PL spectrum blue shifted because of band filling effect, the PL peak at the shorter wavelength of 1208 nm becomes more pronounced. This could be attributed to carrier outflow into the radial InGaAs region with a higher bandgap. The PL peak wavelengths were therefore used to calculate the respective indium composition in different regions without considering quantum well confinement and strain effects. The PL peak wavelengths for the axial InGaAs and radial InGaAs were plotted for different nanowire diameters, as shown in Fig. 1(f). As the nanowire diameter increases, while the axial InGaAs PL peak remains almost unchanged, the radial InGaAs PL peak exhibits a red shift. The red shift can be attributed to either a stronger quantum confinement in the radial quantum wells or varied indium compositions as the diameter increases. To determine the exact cause, however, further investigations using transmission electron microscope are needed. When the same nanowire array which was initially pumped using HeNe CW laser is pumped using a pulsed laser (repletion rate 1 MHz) whose peak power is more than three orders of magnitude higher than the average power of the CW HeNe laser, a significant blue shift in the PL is observed as shown in Fig. 1(e) using the dashed red line plot.

Figure 2(a) shows the top-down view SEM picture of GaAs core nanowire array with an average diameter of 105 nm. The SEM picture of the complete nanowire structure after growing the InGaAs as well as the 15 nm InGaP shell is given in Fig. 2(b), showing increased diameter to 168 nm. We therefore derived the InGaAs radial quantum well thickness to be 16.5 nm, sandwiched between the 15 nm thick InGaP shell and the GaAs core. The schematic of the cross section below the nanowire height of 800 nm is shown in Fig. 2(c).

The nanowires are arranged into a honeycomb lattice with the lattice constant a of 640 nm, diameter of d, and a side length of the hexagon R, as shown in Fig. 2(b). The pattern forms a photonic crystal cavity in which the electromagnetic field oscillates horizontally, with the wavelength selective optical feedback provided by the band edge at Γ-point.[34–39] At the band edge, the group velocity of the light becomes zero and light is diffracted normal to the photonic crystal plane by first order Bragg diffraction, leading to surface emission.[28] Choosing $R = \frac{a}{3}$, the nanowires form a regular hexagon to get undeformed honeycomb lattice as shown at the center of Fig. 2(e). If we choose $R > \frac{a}{3}$, the honeycomb within the unit cell becomes stretched as shown on the left of Fig. 2(e). When $R < \frac{a}{3}$, the honeycomb becomes compressed as shown on the right of Fig. 2(e). To study how the lasing mode of the honeycomb PCSEL changes when the pattern is deformed from its ideal pattern, we design devices with side lengths of the hexagon R of 230, 200, and 210 nm for the stretched, compressed, and undeformed devices, respectively. The fractional deformation factor, calculated as the ratio of the difference between the side lengths of the deformed and undeformed lattices to the side length of undeformed lattice, is 9.5% and 4.7% for the stretched and compressed devices respectively.

To understand the nature of the lasing modes which is the geometry-dependent, wavelength variation, quality factors, and electric field profiles, numerical simulations were performed on the compressed, stretched, and undeformed devices using the finite-difference time-domain (FDTD) method with Asys Lumerical FDTD

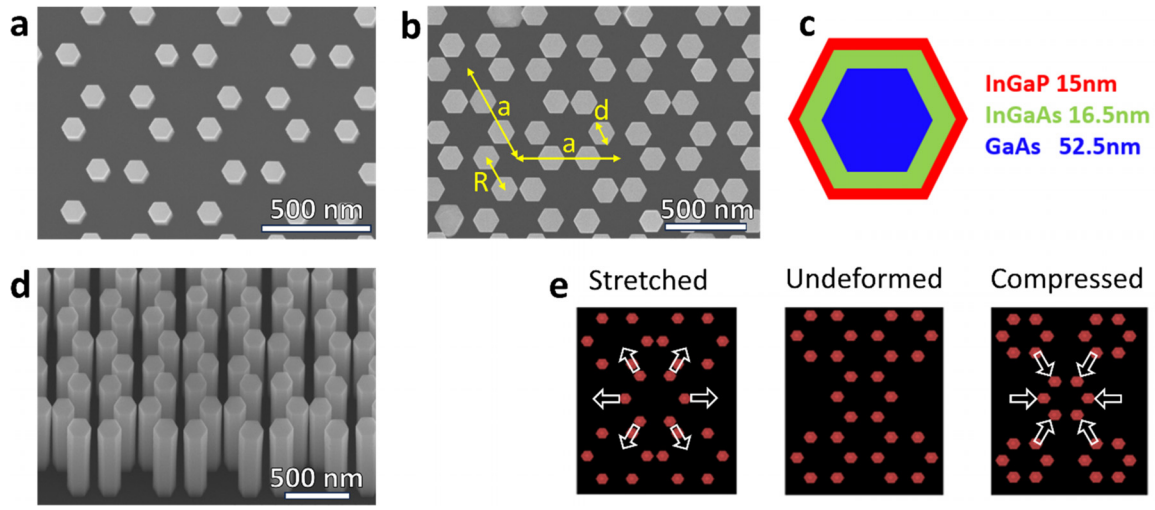

FIG. 2. Top view SEM images showing (a) GaAs core nanowire arrays, (b) a zoomed in view of the complete nanowire array after the InGaP shell was grown indicating the design parameters of the honeycomb PCSEL including the lattice constant a, the diameter of the nanowires d, and the side length of the hexagon R. (c) The schematic of the cross-section view of the nanowires showing the thickness of each layer and the quantum well structure formed. (d) The SEM picture of the honeycomb nanowire arrays (PCSEL) used in this work. (e) The undeformed pattern with $R = \frac{a}{3}$ and stretched $(R > \frac{a}{3})$ and compressed $(R < \frac{a}{3})$ patterns of the honeycomb PCSEL.

simulations[40,41] and guided mode expansion (GME) methods with Legume.[42] In addition to the device parameters mentioned earlier, the simulated devices had the nanowire diameter and height of 168 and 1200 nm, respectively. The FDTD simulation results of the stretched device show that the resonant mode with the highest quality factor ($Q = 1.4 \times 10^6$) is at the wavelength of 984 nm. The top-down view of the electric field profile of the resonant mode is a hexapole as shown in Fig. 3(a), which implies the mode could be a band edge mode. Relating band edge modes in PCSELs with well-defined field patterns including monopole, dipole, quadrupole, and hexapole field profiles was also discussed in Ref. 43. The cross-sectional view of the nanowire showing the field profile of the mode is given on Fig. 3(b). The field is mostly confined within the GaAs core. For this reason, the field interacts mostly with the radial InGaAs well surrounding the core and hence it can use it as the gain material for lasing. The top-down views of the field profile of the lasing modes for the compressed and undeformed devices were also found to be hexapole.

The photonic band diagram of the device obtained using the GME method is shown in Fig. 3(c) using the colors black, blue, and orange for the stretched, compressed, and undeformed devices respectively. For the stretched device, the lasing band edge has the wavelength of 984 nm (shown in the inset), matching the wavelength of the highest quality factor mode presented earlier using the FDTD method. This mode whose field profile was also determined using the GME

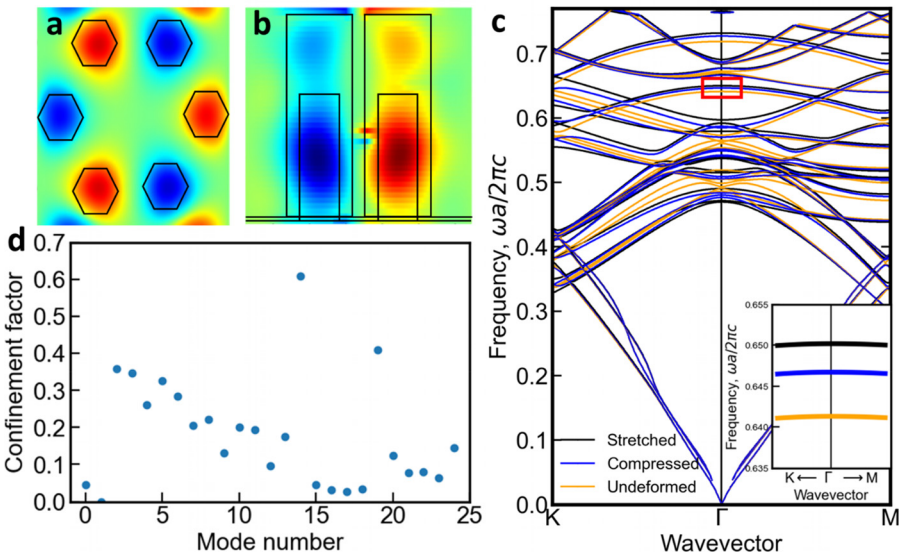

FIG. 3. (a) Top-down view of the electric field profile of the highest quality factor mode for TE polarization calculated by FDTD simulations. (b) The cross-sectional view of the nanowires showing the field profile of the highest quality factor mode. (c) Photonic band diagram of the stretched (black), compressed (blue), and undeformed (orange) devices. The lasing band edges are the Γ-point band edges shown in the inset. (d) Plot of the confinement factor for the 25 modes corresponding to the different bands in the band diagram from the lowest frequency at Γ-point.

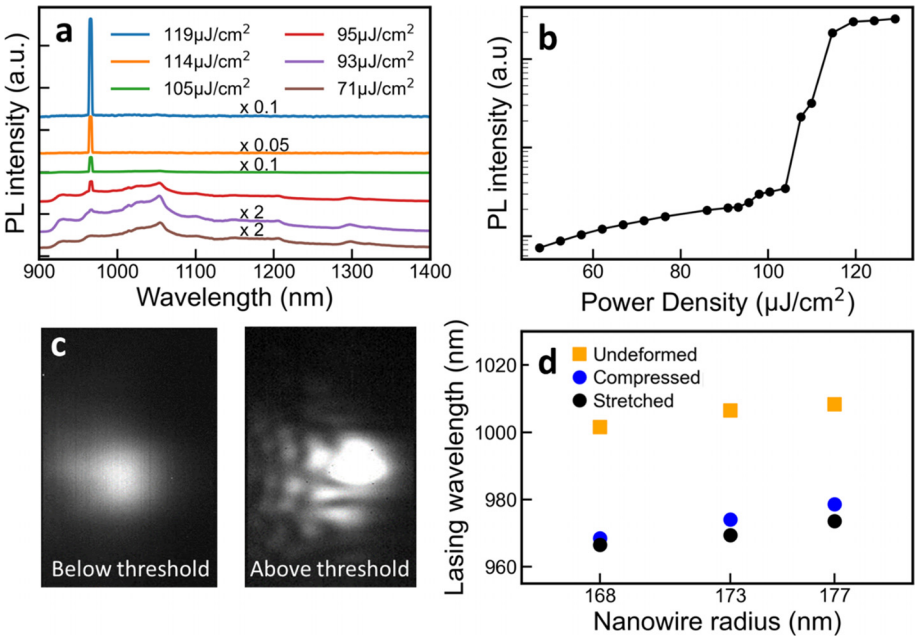

FIG. 4. (a) PL emission spectrum with varied excitations. (b) The plot of light intensity in log scale against pumping power density (L–L curve). (c) Optical image showing the light emission below (left) and above threshold (right). (d) Comparison of the lasing wavelength for different nanowire diameters for the undeformed, compressed, and stretched devices.

method as a hexapole has a good field confinement within the nanowires, with a high confinement factor of about 40%, the second largest of all the modes shown in Fig. 3(d). For each mode, the confinement factor was calculated by taking the sum of the field within the nanowires divided by the sum of the field inside and outside the nanowires. For compressed and undeformed devices, the lasing band edges correspond to the wavelengths of 989 and 1000 nm, respectively.

The stretched honeycomb PCSEL was optically pumped using the pulsed laser source with a beam spot size with a diameter of 12 μm and a pulse width of 100 ps. The wavelength and the repetition rate were set to 633 nm and 1 MHz, respectively. At low pumping powers of 70–90 $\mu J/cm^2$, only spontaneous emission was observed as shown in Fig. 4(a). When the pumping power was increased beyond 103 $\mu J/cm^2$, a lasing peak appeared at the wavelength of 966 nm. As the pumping power is increased beyond the threshold, the intensity of the lasing peak increases. The full width at half maximum of the lasing peak is about 3.7 nm. Figure 4(b) shows the light in vs light out (L–L) curve in log scale. There is a clear threshold at approximately 103 $\mu J/cm^2$. The optical images of the light emission below and above threshold are shown in Fig. 4(c). Figure 4(d) shows a comparison of the lasing wavelength for undeformed, compressed, and stretched devices with different nanowire diameters. For nanowire diameters of 168, 173, and 177 nm, the respective lasing wavelengths are 966, 969, and 973 nm for stretched devices, 968, 974, and 978 nm for compressed devices, and 1001, 1006, and 1008 nm for undeformed devices. The undeformed, compressed, and stretched devices all show a linearly increasing trend in lasing wavelengths with the nanowire diameters. With a greater fractional deformation factor of 9.5%, the stretched device exhibits a shorter lasing wavelength as compared to the compressed one (with a fractional deformation factor of 4.7%). This is consistent with theory in which the more the deformation, the lower the resonance wavelength. The lasing wavelengths agree well with the simulation results in the inset of the band diagram in Fig. 3(c) where the compressed device lasing band edge lies in between that of the stretched and undeformed devices.

In conclusion, we have demonstrated a device that uses radial quantum well in nanowires as the gain material for lasing. The nanowires were grown by MOCVD SAE taking advantage of precise control of nanowire growth position to achieve a nanowire based PCSEL. This work thus demonstrates the potential of using the radially quantum confined nanostructures for energy efficient laser sources integrated on silicon platform.

This work was supported by Engineering and Physical Sciences Research Council (Grant No. EP/S024441/1).

AUTHOR DECLARATIONS

Conflict of Interest

The authors have no conflicts to disclose.

Author Contributions

Balthazar Temu: Conceptualization (lead); Data curation (lead); Formal analysis (equal); Investigation (equal); Methodology (equal); Project administration (lead); Resources (equal); Software (lead); Supervision (lead); Validation (equal); Visualization (equal); Writing – original draft (lead); Writing – review & editing (equal). **Zhao Yan:** Conceptualization (supporting); Data curation (supporting); Formal analysis (lead); Funding acquisition (equal); Investigation (lead); Resources (equal); Validation (lead); Visualization (equal); Writing – review & editing (equal). **Bogdan-Petrin Ratiu:** Data curation (supporting); Investigation (equal); Software (supporting); Validation (equal); Visualization (equal); Writing – review & editing (equal). **Sang Soon Oh:** Conceptualization (supporting); Formal analysis

(equal); Investigation (equal); Methodology (equal); Software (supporting); Supervision (lead); Validation (equal); Visualization (equal); Writing – review & editing (equal). **Qiang Li:** Conceptualization (supporting); Formal analysis (equal); Funding acquisition (lead); Investigation (equal); Methodology (equal); Project administration (supporting); Resources (equal); Supervision (supporting); Validation (equal); Visualization (equal); Writing – review & editing (equal).

DATA AVAILABILITY

The data supporting the findings of this study are available in The Cardiff University Research Portal at https://10.0.66.139/cardiff.27688149.

REFERENCES

[1]K. H. Li, X. Liu, Q. Wang, S. Zhao, and Z. Mi, "Ultralow-threshold electrically injected AlGaN nanowire ultraviolet lasers on Si operating at low temperature," Nat. Nanotechnol. **10**(2), 140–144 (2015).

[2]S. Gradečak, F. Qian, Y. Li, H.-G. Park, and C. M. Lieber, "GaN nanowire lasers with low lasing thresholds," Appl. Phys. Lett. **87**(17), 173111 (2005).

[3]C.-Z. Ning, "Semiconductor nanolasers and the size-energy-efficiency challenge: A review," Adv. Photonics **1**, 014002 (2019).

[4]H. Kim, W.-J. Lee, A. C. Farrell, J. S. D. Morales, P. Senanayake, S. V. Prikhodko, T. J. Ochalski, and D. L. Huffaker, "Monolithic InGaAs nanowire array lasers on silicon-on-insulator operating at room temperature," Nano Lett. **17**(6), 3465–3470 (2017).

[5]W.-J. Lee, H. Kim, A. C. Farrell, P. Senanayake, and D. L. Huffaker, "Nanopillar array band-edge laser cavities on silicon-on-insulator for monolithic integrated light sources," Appl. Phys. Lett. **108**(8), 081108 (2016).

[6]E. Ertekin, P. A. Greaney, D. C. Chrzan, and T. D. Sands, "Equilibrium limits of coherency in strained nanowire heterostructures," J. Appl. Phys. **97**(11), 114325 (2005).

[7]P. Caroff, K. A. Dick, J. Johansson, M. E. Messing, K. Deppert, and L. Samuelson, "Controlled polytypic and twin-plane superlattices in III-V nanowires," Nat. Nanotechnol. **4**(1), 50–55 (2009).

[8]M. Fox, *Optical Properties of Solids*, 2nd ed. (Oxford University Press, Oxford, 2012).

[9]H. J. Joyce, Q. Gao, H. Hoe Tan, C. Jagadish, Y. Kim, J. Zou, L. M. Smith, H. E. Jackson, J. M. Yarrison-Rice, P. Parkinson, and M. B. Johnston, "III–V semiconductor nanowires for optoelectronic device applications," Prog. Quantum Electron. **35**(2), 23–75 (2011).

[10]P. Parkinson, H. J. Joyce, Q. Gao, H. H. Tan, X. Zhang, J. Zou, C. Jagadish, L. M. Herz, and M. B. Johnston, "Carrier lifetime and Mobility enhancement in nearly defect-free core−shell nanowires measured using time-resolved terahertz spectroscopy," Nano Lett. **9**(9), 3349–3353 (2009).

[11]G. Zhang, M. Takiguchi, K. Tateno, T. Tawara, M. Notomi, and H. Gotoh, "Telecom-band lasing in single InP/InAs heterostructure nanowires at room temperature," Sci. Adv. **5**(2), eaat8896 (2019).

[12]M. Notomi, M. Takiguchi, S. Sergent, G. Zhang, and H. Sumikura, "Nanowire photonics toward wide wavelength range and subwavelength confinement [Invited]," Opt. Mater. Express **10**(10), 2560–2596 (2020).

[13]N. I. Goktas, V. G. Dubrovskii, and R. R. LaPierre, "Conformal growth of radial InGaAs quantum wells in GaAs nanowires," J. Phys. Chem. Lett. **12**(4), 1275–1283 (2021).

[14]K. Nakama, M. Yukimune, N. Kawasaki, A. Higo, S. Hiura, A. Murayama, M. Jansson, W. M. Chen, I. A. Buyanova, and F. Ishikawa, "GaAs/GaInNAs core-multishell nanowires with a triple quantum-well structure emitting in the telecommunication range," Appl. Phys. Lett. **123**(8), 081104 (2023).

[15]J. Jadczak, P. Plochocka, A. Mitioglu, I. Breslavetz, M. Royo, A. Bertoni, G. Goldoni, T. Smolenski, P. Kossacki, A. Kretinin, H. Shtrikman, and D. K. Maude, "Unintentional high-density p-type modulation doping of a GaAs/AlAs core–multishell nanowire," Nano Lett. **14**(5), 2807–2814 (2014).

[16]P. Schmiedeke, A. Thurn, S. Matich, M. Döblinger, J. J. Finley, and G. Koblmüller, "Low-threshold strain-compensated InGaAs/(In,Al)GaAs multi-quantum well nanowire lasers emitting near 1.3 μm at room temperature," Appl. Phys. Lett. **118**(22), 221103 (2021).

[17]S. Adhikari, F. Kremer, M. Lysevych, C. Jagadish, and H. H. Tan, "Core–shell GaN/AlGaN nanowires grown by selective area epitaxy," Nanoscale Horiz. **8**(4), 530–542 (2023).

[18]W. W. Wong, S. Church, C. Jagadish, N. Wang, P. Parkinson, and H. H. Tan, "Selective area epitaxy of InP/InAsP multi-quantum well micro-ring lasers," in *IEEE Photonics Conference (IPC)* (IEEE, 2022), pp. 1–2.

[19]G. Koblmüller and G. Abstreiter, "Growth and properties of InGaAs nanowires on silicon," Phys. Status Solidi RRL **8**(1), 11–30 (2014).

[20]J. Noborisaka, J. Motohisa, and T. Fukui, "Catalyst-free growth of GaAs nanowires by selective-area metalorganic vapor-phase epitaxy," Appl. Phys. Lett. **86**(21), 213102 (2005).

[21]K. Tomioka, K. Ikejiri, T. Tanaka, J. Motohisa, S. Hara, K. Hiruma, and T. Fukui, "Selective-area growth of III-V nanowires and their applications," J. Mater. Res. **26**(17), 2127–2141 (2011).

[22]B.-P. Ratiu, B. Temu, C. Messina, O. Abouzaid, S. Rihani, G. Berry, S. S. Oh, and Q. Li, "Curved InGaAs nanowire array lasers grown directly on silicon-on-insulator," Opt. Express **31**(22), 36668–36676 (2023).

[23]H. Kim, W.-J. Lee, T.-Y. Chang, and D. L. Huffaker, "Room-temperature InGaAs nanowire array band-edge lasers on patterned silicon-on-insulator platforms," Phys. Status Solidi RRL **13**(3), 1800489 (2019).

[24]W.-J. Lee, H. Kim, J.-B. You, and D. L. Huffaker, "Ultracompact bottom-up photonic crystal lasers on silicon-on-insulator," Sci. Rep. **7**(1), 9543 (2017).

[25]J. Treu, M. Bormann, H. Schmeiduch, M. Döblinger, S. Morkötter, S. Matich, P. Wiecha, K. Saller, B. Mayer, M. Bichler, M.-C. Amann, J. J. Finley, G. Abstreiter, and G. Koblmüller, "Enhanced luminescence properties of InAs–InAsP core–shell nanowires," Nano Lett. **13**(12), 6070–6077 (2013).

[26]M. H. Sun, H. J. Joyce, Q. Gao, H. H. Tan, C. Jagadish, and C. Z. Ning, "Removal of surface states and recovery of band-edge emission in InAs nanowires through surface passivation," Nano Lett. **12**(7), 3378–3384 (2012).

[27]J. W. W. van Tilburg, R. E. Algra, W. G. G. Immink, M. Verheijen, E. P. A. M. Bakkers, and L. P. Kouwenhoven, "Surface passivated InAs/InP core/shell nanowires," Semicond. Sci. Technol. **25**(2), 024011 (2010).

[28]J. Treu, T. Stettner, M. Watzinger, S. Morkötter, M. Döblinger, S. Matich, K. Saller, M. Bichler, G. Abstreiter, J. J. Finley, J. Stangl, and G. Koblmüller, "Lattice-matched InGaAs–InAlAs core–shell nanowires with improved luminescence and photoresponse properties," Nano Lett. **15**(5), 3533–3540 (2015).

[29]Y. Dan, K. Seo, K. Takei, J. H. Meza, A. Javey, and K. B. Crozier, "Dramatic reduction of surface recombination by in situ surface passivation of silicon nanowires," Nano Lett. **11**(6), 2527–2532 (2011).

[30]C. Messina, Y. Gong, O. Abouzaid, B.-P. Ratiu, T. Grieb, Z. Yan, A. Rosenauer, S. S. Oh, and Q. Li, "Deformed honeycomb lattices of InGaAs nanowires grown on silicon-on-insulator for photonic crystal surface-emitting lasers," Adv. Opt. Mater. **11**(5), 2201809 (2023).

[31]Y.-H. Ra, R. T. Rashid, X. Liu, S. Md. Sadaf, K. Mashooq, and Z. Mi, "An electrically pumped surface-emitting semiconductor green laser," Sci. Adv. **6**(1), eaav7523 (2020).

[32]M. F. Vafadar and S. Zhao, "Ultralow threshold surface emitting ultraviolet lasers with semiconductor nanowires," Sci. Rep. **13**(1), 6633 (2023).

[33]S. Ishizawa, K. Kishino, R. Araki, A. Kikuchi, and S. Sugimoto, "Optically pumped green (530–560 nm) stimulated emissions from InGaN/GaN multiple-quantum-well triangular-lattice nanocolumn arrays," Appl. Phys. Express **4**(5), 055001 (2011).

[34]T. Inoue, M. Yoshida, J. Gelleta, K. Izumi, K. Yoshida, K. Ishizaki, M. De Zoysa, and S. Noda, "General recipe to realize photonic-crystal surface-emitting lasers with 100-W-to-1-kW single-mode operation," Nat. Commun. **13**(1), 3262 (2022).

[35]T. Inoue, M. Yoshida, M. D. Zoysa, K. Ishizaki, and S. Noda, "Design of photonic-crystal surface-emitting lasers with enhanced in-plane optical feedback for high-speed operation," Opt. Express **28**(4), 5050–5057 (2020).

[36]S. Noda, T. Inoue, M. Yoshida, J. Gelleta, M. D. Zoysa, and K. Ishizaki, "High-power and high-beam-quality photonic-crystal surface-emitting lasers: A tutorial," Adv. Opt. Photonics **15**(4), 977–1032 (2023).

[37]K. Sakai, E. Miyai, T. Sakaguchi, D. Ohnishi, T. Okano, and S. Noda, "Lasing band-edge identification for a surface-emitting photonic crystal laser," IEEE J. Sel. Areas Commun. **23**(7), 1335–1340 (2005).
[38]D. Ohnishi, T. Okano, M. Imada, and S. Noda, "Room temperature continuous wave operation of a surface-emitting two-dimensional photonic crystal diode laser," Opt. Express **12**(8), 1562–1568 (2004).
[39]S. Noda, K. Kitamura, T. Okino, D. Yasuda, and Y. Tanaka, "Photonic-crystal surface-emitting lasers: Review and introduction of modulated-photonic crystals," IEEE J. Sel. Top. Quantum Electron. **23**(6), 1–7 (2017).
[40]Ansys Optics, "Finite difference time domain (FDTD) solver introduction," available at https://www.ansys.com/en-gb/blog/what-is-fdtd.
[41]A. Taflove and S. Hagness, *Computational Electrodynamics: The Finite-Difference Time-Domain Method*, 2nd ed. (Artech House, 2000).
[42]S. Zanotti, M. Minkov, D. Nigro, D. Gerace, S. Fan, and L. C. Andreani, "Legume: A free implementation of the guided-mode expansion method for photonic crystal slabs," Comput. Phys. Commun. **304**, 109286 (2024).
[43]M. Imada, A. Chutinan, S. Noda, and M. Mochizuki, "Multidirectionally distributed feedback photonic crystal lasers," Phys. Rev. B **65**(19), 195306 (2002).